Light Extraction of Trapped Optical Modes in Polymer Light-Emitting Diodes with Nanoimprinted Double-Pattern Gratings

Lei Zhou,[†] Xiaochen Jiang,[†] Yanqing Li,*[,†] Aili Shi,[†] Jingde Chen,[†] Qingdong Ou,[†] Haitao Liu,[‡] and Jianxin Tang*[,†]

[†]Institute of Functional Nano and Soft Materials (FUNSOM), Jiangsu Key Laboratory for Carbon-Based Functional Materials and Devices, Collaborative Innovation Center of Suzhou Nano Science and Technology, Soochow University, Suzhou 215123, China

[‡]Key Laboratory of Optical Information Science and Technology, Ministry of Education, Institute of Modern Optics, Nankai University, Tianjin 300071, China

Ⓢ *Supporting Information*

ABSTRACT: Despite the rapid development of polymer light-emitting diodes (PLEDs), the overall device efficiency is still limited because ∼80% of the generated light is trapped in a conventional device architecture by the high refractive index of organic materials and the optical confinement and internal reflection. The implementation of the energy dissipation compensation techniques is urgently required for further enhancement in the efficiency of PLEDs. Here, we demonstrate that incorporating the double-pattern Bragg gratings in the organic layers with soft nanoimprinting lithography can dramatically enhance the light extraction of trapped optical modes in PLEDs. The resulting efficiency is 1.35 times that of a conventional device with a flat architecture

used as a comparison. The experimental and theoretical analyses indicate that the enhanced out-coupling efficiency is attributed to the combination of the ordinary Bragg scattering, the guided-mode resonance (GMR), surface plasmon polariton (SPP) modes, and the hybrid anticross coupling between GMR and SPP, leading to the extraordinary efficient photo flux that can transfer in direction of the leaky modes. We anticipate that our method provides a new pathway for precisely manipulating nanoscale optical fields and could enable the integration of different optical modes in PLEDs for the viable applications.

KEYWORDS: polymer light-emitting diodes, optical grating, light extraction, leaky modes, guided-mode resonance
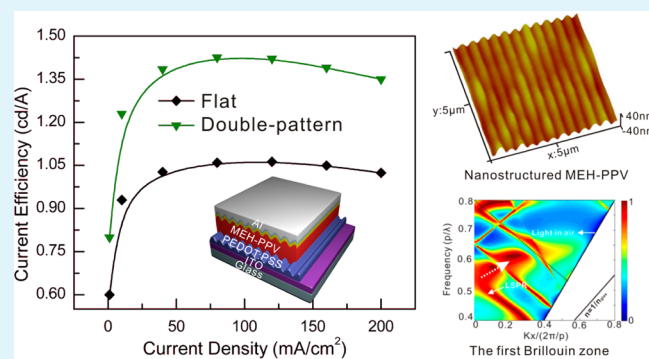
1. INTRODUCTION

The development of solution-processed conjugated polymer light-emitting diodes (PLEDs) holds great promise for the production of large-area, high-resolution flat panel displays, solid-state lighting source, and flexible displays because of their steadily improved efficiency and superior color quality, together with desirable features such as fast response and continuous brightness control.[1−3] In recent years, PLEDs with an internal quantum efficiency (IQE) of approaching 100% have been realized due to the use of phosphorescent or thermally activated delayed fluorescent emitters for the energy conversion of both the singlet and triplet states.[4,5] However, in conventional PLEDs constructed in a standard substrate emitting architecture, the out-coupling efficiency is approximately 20%, and the majority of the light generated in the organic layers is confined in the waveguide (WG) mode, surface plasmon polaritons (SPP) mode, and substrate mode due to the large difference in the refractive indices n between active organic/transparent indium tin oxide (ITO) layers ($n_{org} \approx 1.75$, $n_{ITO} \approx 1.8$) and the glass substrate ($n_{glass} \approx 1.45$).[6−8] Consequently, the greatest

potential for a substantial increase in the device efficiency of PLEDs is to enhance the light out-coupling.

Many advanced techniques have been studied for extracting the confined light in PLEDs, such as microlens arrays,[9,10] light scattering centers,[11] Bragg mirrors,[12] periodic corrugation,[13] embedded low-index dielectric grid,[14,15] photonic crystals,[16] antireflection coatings,[17,18] wrinkles,[19] and periodic metallic grating electrode based on plasmonic effect.[20−23] However, there are still some obstacles for some of these extraction approaches in the applications of solution-processed PLEDs. Particularly, it is highly desirable to avoid the complicated and hence unacceptably high-cost fabrication procedures.

Here, we present a universal method for highly efficient light extraction of trapped optical modes in PLEDs by introducing the double-patterned Bragg gratings into the organic layers via soft nanoimprinting lithography, which is fully compatible with the low-temperature solution process. In the devices, the

optimum one-dimensional Bragg grating is incorporated into both hole transporting layer of poly(styrenesulfonate)-doped poly(3,4-ethylenedioxythiophene) (PEDOT:PSS) and polymer emitting layer of poly(2-methoxy-5-(2′-ethyl-hexyloxy)-1,4-phenylenevinylene) (MEH-PPV), enabling a double-deck corrugated structure. The resulting efficiency is 1.35 times that of a conventional device with a flat architecture. The experimental and theoretical analyses indicate that the enhanced out-coupling efficiency is attributed to the extraction of the trapped light from both ITO/organic interface and organic/metal interface. Besides ordinary Bragg scattering, the guided-mode resonance (GMR) and the hybrid interactions of different optical modes are also devoted to the extraordinary efficient photo flux in nanostructure-based PLEDs, which can transfer in direction of the leaky modes and yield out-coupling efficiency enhancement.

2. EXPERIMENTAL DETAILS

2.1. Fabrication Procedures. The fabrication process of PDMS molds and corrugated PLEDs is schematically shown in Figure 1. First,
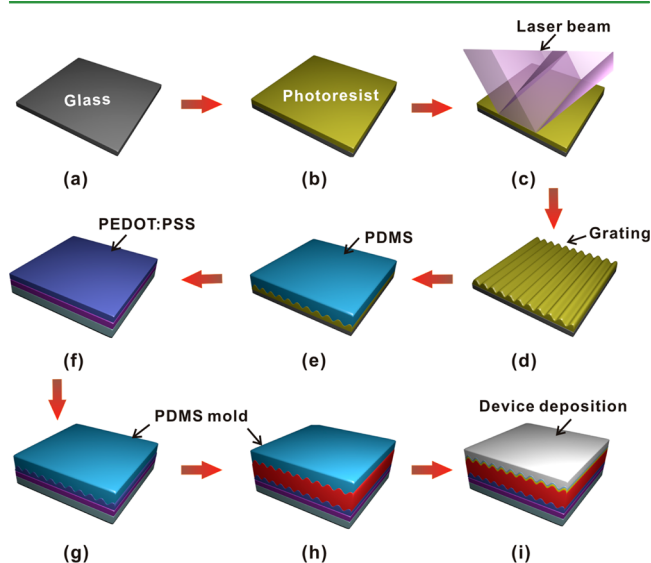
Figure 1. Schematic of the fabrication process of corrugated PLEDs. (a) Cleaning the glass substrate. (b) Spin-coating the photoresist on glass substrate. (c) Holographic photolithography. (d) Developing and the grating formation on photoresist. (e) Fabricating PDMS mold from the grating-structured photoresist film. (f) Spin-coating the PEDOT:PSS layer on precleaned ITO glass substrate. (g) Imprinting the PEDOT:PSS layer by grating-structured PDMS mold. (h) Imprinting the MEH-PPV layer spin-coated on patterned PEDOT:PSS substrate. (i) Depositing organic layers and metal electrode to complete the device fabrication.

the glass was cleaned with acetone, isopropyl alcohol, and distilled water for 10 min and dried in the air. Then, the photoresist (RZJ390PG, SUZHOU RUIHONG CO. Ltd.) with the thickness of 600 nm was spin-coated onto the glass substrate and baked for 80 s at 100 °C. After exposing for 2 s with a laser beam (441 nm, He–Cd), the samples were developed in NaOH (0.4%) solution for 4 s and dried in the air. As a result, one-dimensional (1D) grating with a 320 nm period, 0.6 duty cycle, 400 nm groove depth (see Supporting Information Figure S1) was fabricated on the surface of the photoresist film. Thereafter, poly(dimethyl-siloxane) (PDMS premixed with 1/10 cross-linker, both from Dow Corning Co.) was poured on the surface of surface-relief photoresist grating and taken into vacuum oven annealing for 2 h at 60 °C. Subsequently, the PDMS mold was peeled off from the photoresist. These grating structures were inscribed into

PLEDs by the method of soft nanoimprinting lithography technology.[24,25]

2.2. Device Fabrication. The PLEDs were fabricated on ITO-coated glass substrates with a sheet resistance of 20 Ω sq^{-1} and the ITO thickness is around 120 nm. Prior to the device fabrication, the ITO glass substrates were ultrasonically cleaned with detergent, acetone, ethanol, and DI water for 20 min and finally dried in an oven. The PEDOT:PSS was spin-coated onto the ultraviolet-ozone (UVO) treated ITO glass substrates under ambient condition, which was used as a hole transport layer (HTL). After imprinting the PEDOT:PSS layer, the samples were transferred into a nitrogen-filled glovebox to prepare the MEH-PPV (8 mg/mL, dissolved in p-xylene) by spin-coating. The gratings were also incorporated into the MEH-PPV film by the same nanoimprinting techniques. Finally, to complete the device, an electron transport layer (ETL) of 4,7-diphenyl-1,10-phenanthroline (BPhen) (3 nm) and a bilayer cathode of lithium fluoride (LiF, 1 nm)/aluminum (Al, 100 nm) were deposited by thermal evaporation in a high vacuum system with a base pressure of 2 × 10^{-6} Torr. The effective device area was 0.1 cm^2.

2.3. Characterizations. The current density–voltage–luminance (J–V–L) characteristics of the corresponding devices were measured simultaneously using a computer-controlled programmable Keithley model 2400 power source and a PhotoResearch PR 655 spectrometer. The angle-dependent emission intensity was measured by placing the devices on a rotation stage with one of the grooves parallel to the rotation axis. Surface morphology was characterized with atomic force microscopy (AFM) (Veeco MultiMode V) in tapping mode. The thickness, refractive index (n), and extinction coefficient (k) of all the films were measured using the α-SE Spectroscopic Ellipsometer (J.A. Woollam Co., Inc.). Transmission spectra were recorded by an UV/vis/near-IR spectrophotometer (PerkinElmer Lambda 750) with the integrating sphere.

2.4. Theoretical Modeling. To study the optical properties of the corrugated PLEDs, a rigorous electromagnetic analysis based on the rigorous coupled wave analysis (RCWA) was adopted to calculate dispersion diagram as well as the near-field distribution of the PLEDs based on the optical calculation (Rsoft DiffractMOD) with commercial RSoft 8.1 (RSoft Design Group, Inc.) and corresponding codes generated in-house. In the modeling, the complex optical dielectric function of the nanostructured Al cathode was fitted using the Drude–Lorentz model, taking into account interband transitions. The frequency-dependent refractive index (n) and extinction cofficient (k) of PEDOT:PSS and MEH-PPV measured experimentally by ellipsometer were used as experimtal input parameters for calculation (see Supporting Information Figure S2).

3. RESULTS AND DISCUSSION

3.1. Device Structure. The schematic structures of PLEDs with four structures are shown in Figure 2, which was constructed with a configuration of ITO-glass/PEDOT:PSS/MEH-PPV/BPhen/LiF/Al. Here, the ITO coated glass is used as a transparent anode and the LiF/Al as the cathode. The PEDOT:PSS and BPhen act as HTL and ETL, respectively, to improve the injection and transport of holes and electrons. MEH-PPV was selected as an emission layer due to the advantages of its soluble ability in the conjugated form and compatibility with soft nanoimpriting process.[26,27]

To obtain the optimum grating structure for efficient light extraction in PLEDs, the extraordinary optical absorption spectra were calculated as a function of light wavelength, the period and duty cycle of the grating. The modeling was based on the opinion that the enhanced transmission and the extraordinary optical absorption can attribute to the same resonant optical mode in the structure.[28−30] According to the calculated results in Figure 3, it is easy to find that the optimum grating should possess a period of ~320 nm and a duty cycle of ~0.6, which is favorable for highly efficient light extraction.
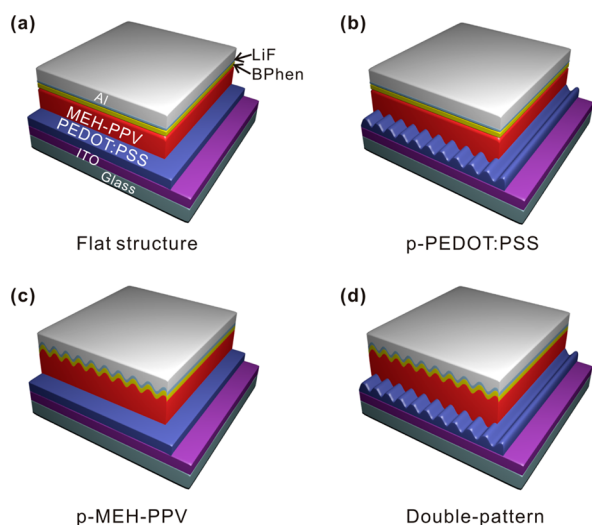
Figure 2. Schematic illuminations of device structures with (a) flat structure, (b) patterned grating on the PEDOT:PSS layer (p-PEDOT:PSS), (c) patterned grating on the MEH-PPV layer (p-MEH-PPV), and (d) double-patterned grating (double-pattern).
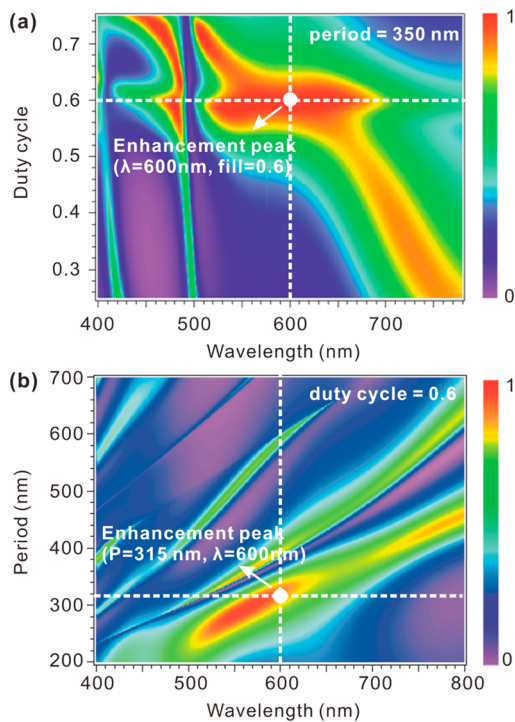
Figure 3. Simulations of the wavelength dependence of extraordinary optical absorption enhancement based on grating parameters: (a) duty cycle and (b) grating period.

The AFM measurements were performed to clarify the morphology change of the PEDOT:PSS and MEH-PPV layers before and after nanoimprinting. It is evident that the surface morphologies of the PEDOT:PSS layer spin-coated on ITO-glass substrate (Figure 4a) and the MEH-PPV on unpatterned (Figure 4c) and patterned PEDOT:PSS layers (Figure 4e) are rather smooth, and their root-mean-square (RMS) roughnesses are approximately 1.05 ± 0.1 nm. Particularly, the AFM image in Figure 4e suggests that the underlying PEDOT:PSS layer with imprinted gratings has no significant influence on the morphology of the upper MEH-PPV. On the contrary, it is
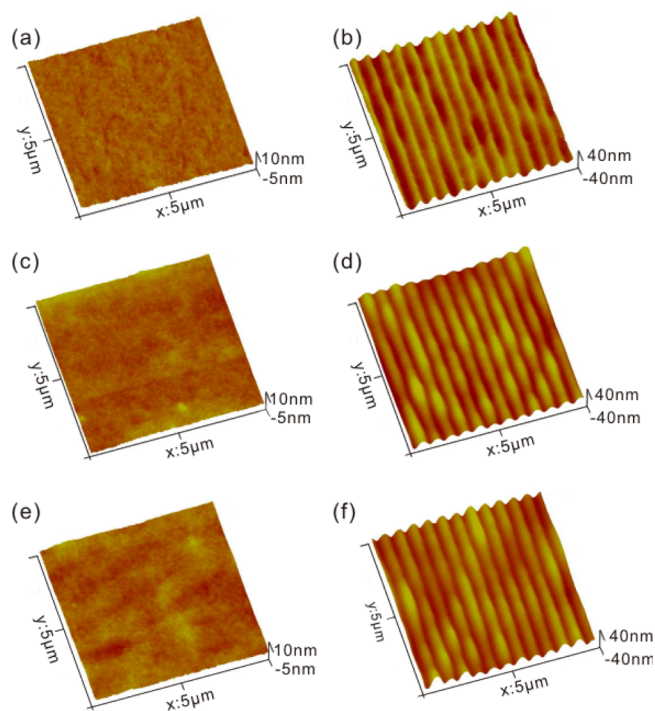

Figure 4. Atomic force microscopy (AFM) images of (a) the flat PEDOT:PSS layer, (b) the patterned PEDOT:PSS layer on ITO-glass substrate, (c) the spin-coated MEH-PPV layer on flat PEDOT:PSS substrate, (d) the patterned MEH-PPV layer on flat PEDOT:PSS substrate, (e) the spin-coated MEH-PPV layer on patterned PEDOT:PSS substrate, and (f) the patterned MEH-PPV layer on patterned PEDOT:PSS substrate. The patterning structure of both PEDOT:PSS and MEH-PPV is same, showing an approximate period of 320 nm, a groove depth of ~40 nm, and a duty cycle of 0.6.

obvious that the well-designed 1D Bragg grating patterns have been transferred to the surface of PEDOT:PSS and MEH-PPV layers by soft nanoimprinting technique using PDMS mold (see Figure 4b, d, and f). A uniform grating structure on PEDOT:PSS and MEH-PPV comprising smooth corrugation is formed, and the morphology of the imprinted MEH-PPV is almost identical to that of the patterned PEDOT:PSS, showing a well-defined groove depth of 40 nm and duty cycle of 0.6.

In addition, as shown in Supporting Information Figure S3, the percentage of transmitted light that is scattered, which is also called haze [haze = (total transmittance-specular transmittance)/total transmittance],[31] for patterned organic layers on ITO-glass substrates is also characterized. It is evident that scattering is present and contributes to the total transmission in the corrugated PLEDs, indicating that the grating structures enable the omnidirectional light out-coupling in patterned PLEDs.

3.2. Device Performance Characteristics. The performance characteristics of PLEDs with four different structures (as illuminated in Figure 2) are compared on plotted in Figure 5. The current density−voltage (J−V) curves in Figure 5a show that the electrical properties of devices with patterns are almost identical to that with a flat structure, and the subtle difference in the curves can be attributed to the slight variation in the layer thickness of a corrugated structure.[19,32] However, the current efficiency of the PLEDs with patterned structures are dramatically increased compared to that with a flat structure. For example, the current efficiency of the device with only a patterned PEDOT:PSS layer (hereafter termed as p-
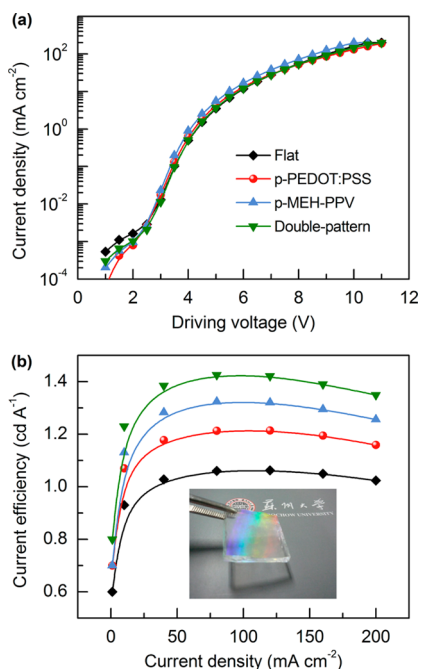
Figure 5. (a) Current density−voltage (J−V) characteristics and (b) current efficiency as a function of current density of PLEDs with four device structures. Inset in part b shows a photograph of the grating-structured PDMS mold.

Figure 6. Normalized emission spectra of PLEDs at a viewing-angle of (a) 0° and (b) 30°. Inset in (a) shows the photography of the flat and double-pattern devices operated at the same bias voltage.

PEDOT:PSS) is 1.21 cd A^{-1} at a current density of 80 mA cm^{-2}, which is 14% enhanced than that of the device with a flat structure (hereafter termed as Flat, 1.06 cd A^{-1}). The PLED with only a patterned MEH-PPV layer (hereafter termed as p-MEH-PPV) exhibits a current efficiency of 1.32 cd A^{-1}, which is 25% higher than that of the Flat device. Moreover, the patterning of both PEDOT:PSS and MEH-PPV (hereafter termed as double-pattern) enables a further enhancement in efficiency by a factor of 1.35 times that of the Flat one, and the resulting double-pattern device yields a maximum current efficiency of 1.43 cd A^{-1}. The external quantum efficiency (EQE) of the corresponding four devices is also characterized (see Supporting Information Figure S4). The EQE of the double-pattern device is around 32% higher than that of the Flat one. Note that the enhancement ratio of the EQE is slightly lower than that of the current efficiency in normal emission, which could be attributed to the slight decrease in electroluminescent (EL) intensity with the increase in viewing angle.[33]

To evaluate the influence of the grating structure on the spectral distribution, the angular dependence of the electroluminescent (EL) spectra is measured from the experimental devices at the viewing angles of 0° and 30° relative to the surface normal. It is clear in Figure 6 that the EL spectrum of the Flat device shows a peak at 600 nm, which corresponds to the emission of MEH-PPV.[34,35] Moreover, the normalized EL spectra of the p-PEDOT:PSS, p-MEH-PPV, and double-pattern devices are, to some extent, different from the Flat one, and the shoulder peak around ~640 nm was obviously enhanced. The difference in the EL spectra with respect to the viewing angle indicate that the periodic corrugated structure parameter influences the spectral characteristics.[36,37]

3.3. Theoretical Calculation. In the previous reports,[22,23,38−41] the efficiency enhancement with the adoption of a periodic nanostructure in organic LEDs or PLEDs is simply
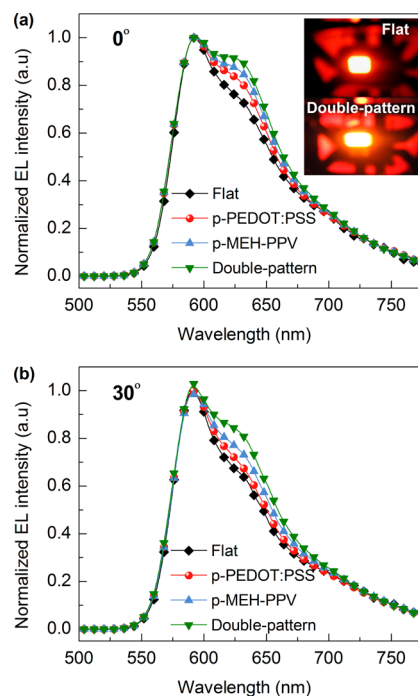
attributed to Bragg scattering produced by the photonic structure, or SPP modes associated with cavity modes. However, Bragg scattering alone or coupling between SPP and cavity modes cannot perfectly explain the EL spectra peak shape change in the periodic corrugated devices. In addition, the hybrid interactions of different optical modes, such as WG, GMR, and SPP modes are also believed to influence the performance of the devices. Therefore, to explain the current efficiency enhancement and EL spectra variation, all of these factors must be considered. Here, we carried out a rigorous electromagnetic analysis based on the RCWA method to identify the nature of these optical modes in the corrugated devices. The dispersion diagrams for both transverse electric (TE) and transverse magnetic (TM) polarized lights were calculated as a function of frequency and in plane wave vector k_x in the first Brillouin zone of p-PEDOT:PSS, p-MEH-PPV, and double-pattern devices. As shown in Figure 7, optical modes can be clearly observed in the first Brillouin zone of devices, and the photo flux with different intensities is tuned with the patterned nanostructures in the devices. The useful light region (leaky mode for light to escape from the device) is located above the line that is named light in air ($k_x/(2\pi/P) < k_0$). The region below the light in air and above the light in glass is the trapped light region, corresponding to the waveguide modes ($k_x/(2\pi/P) > k_0$).[42] The calculated dispersion diagrams in Figure 7 turn out that the p-PEDOT:PSS device enables the efficient photo flux transfer from GMR modes of both TE and TM polarized lights to leaky modes, radiating into far-field with tight-mode confinement without any other coupling.[43] It is an important factor for the efficiency enhancement and the variation in EL spectra of the p-PEDOT:PSS device except for the Bragg scattering.

With the introduction of a periodic grating, the in-plane wavevectors between the SPP modes follow the equation:
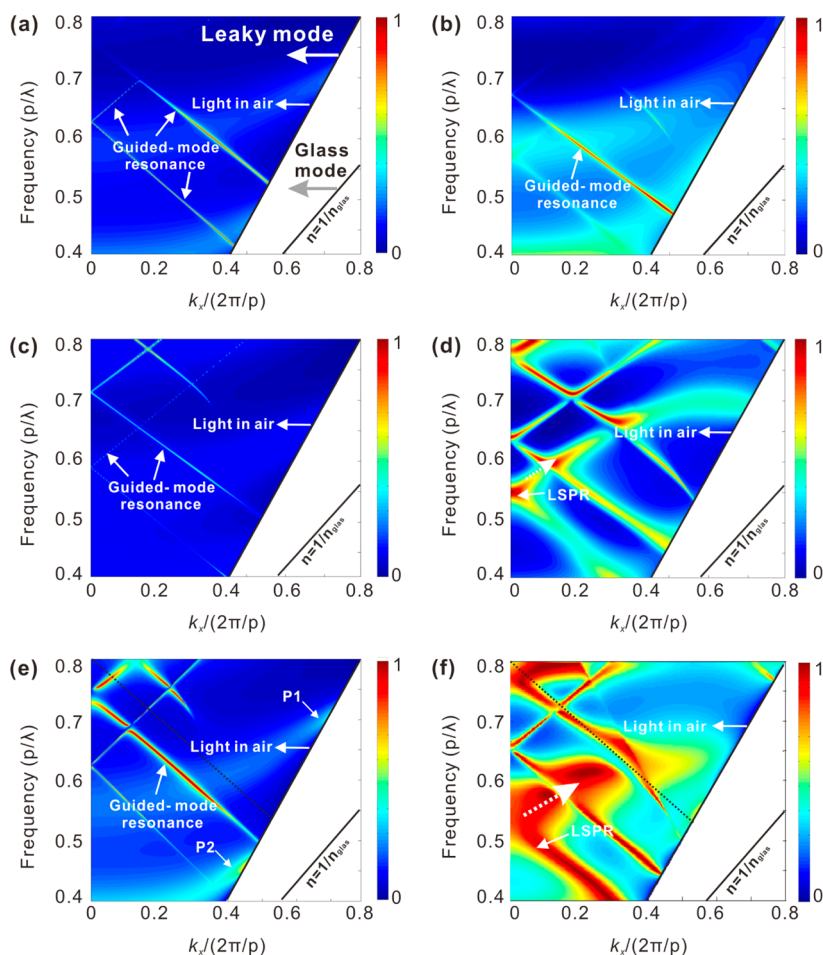
Figure 7. Calculated dispersion diagrams as a function of frequency and in plane wave vector k_x in the first Brillouin zone for (a) TE and (b) TM polarized lights in the device with p-PEDOT:PSS, for (c) TE and (d) TM polarized lights in the device with p-MEH-PPV, and for (e) TE and (f) TM polarized lights in the device with double-pattern. The black line is light line for $n = 1$, and the large white dashed arrows indicate the propagation direction of the hybrid constructive interference between GMR and SPP modes.

$$\frac{k_0}{G}\sin\theta = \frac{k_{spp}}{G} + m \tag{1}$$

where k_0 and k_{spp} are the in-plane wavevectors of the light in air and the SPPs, respectively, G ($= 2\pi/P$) is the lattice vector, and m is an integer that depicts the order of the coupling process. As previously displayed in Figure 3, the enhancement peak of the extraordinary optical absorption will occur at a specific resonant frequency, which enables the interaction of GMR and SPP modes to overcome their momentum mismatch, providing a route to transport into leaky modes and to be scattered into air. For the p-MEH-PPV PLED (Figure 7d), the plane wave can couple to SPPs at the organic/Al interface at a specific resonant frequency ~0.5 (at a wavelength of 640 nm). Meanwhile, it is shown that a hybrid anticross coupling between the SPPs and GMR originated from Al grating occurs, enabling the useful photon flux transfer to far-field with low propagation loss due to the tight-mode confinement.[44] More importantly, the hybrid coupling does shift and split at a frequency of 0.55 ($P/\lambda =$ 0.55), leading to an intriguing modification of the interaction among GMR, SPPs, and waveguide modes, which ultimately couples into the leaky modes for light transmission out of the glass side in the air ($n = 1$) more efficiently. The large white dashed arrow in Figure 7d depicts the propagation direction of the hybrid interference between SPPs and GMR.[45,46]

Remarkably, the intensities of GMR, SPP and their hybrid anticross coupling can be further enhanced for the double-pattern device, as shown in Figure 7e and f. The hybrid resonant wavelength can cross large angles, which is consistent with EL performance, as shown in Figure 6. The reason is attributed to the presence of intertwined interaction between PEDOT:PSS grating and corrugated Al grating, which is accompanied by the change of optical impedance of both PEDOT:PSS ($n = 1.46$) and MEH-PPV emission layer ($n = 1.75$). Compared to the case of TM polarized light, the SPPs cannot be excited by TE polarized light for 1D metallic grating as shown in Figure 7a, c, and e. However, as discussed above, the TE modes of GMR can transfer to leaky modes, which will effectively improve the out-coupling of trapped light into air. This evidence illustrates that the incorporation of grating structures into PLEDs can significantly influence the optical field distribution and thereby the light extraction. Additionally, Figure 7e shows that two sharp photo flux regions P1 and P2 originating from the periodic interference modulation of the double-pattern gratings can also become leaky modes so as to have a significant influence on the EL spectra.[47,48]

To gain further insight into the optical manipulation of light in PLEDs with the grating patterns, we perform the optical modeling calculations of light propagation using the finite-difference-time-domain (FDTD) method. Figure 8 displays the
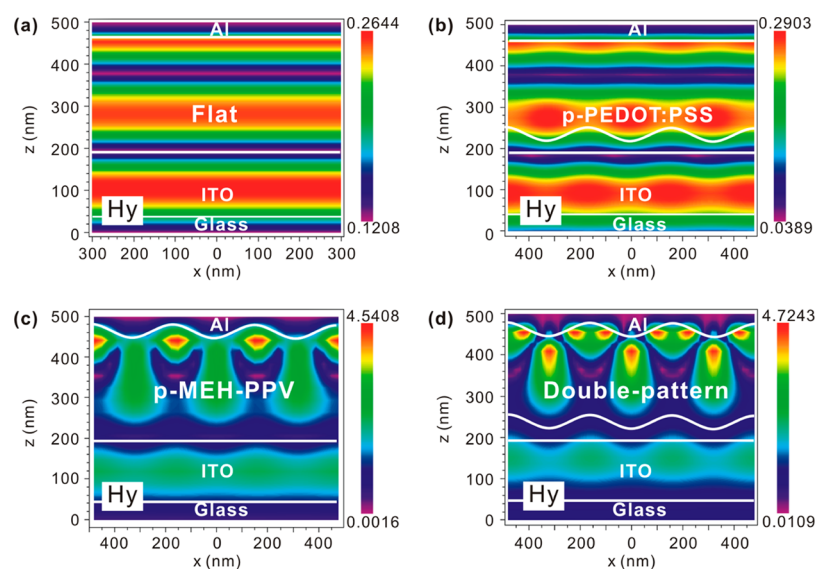
Figure 8. Simulation of near-field distributions of the magnetic field intensity Hy at a wavelength of 640 nm (frequency = 0.5) for four device structures with (a) Flat, (b) p-PEDOT:PSS, (c) p-MEH-PPV, and (d) double-pattern. The simulation was performed by illuminating the devices with an external far-field plan wave.

cross-section field profiles of the magnetic field intensity Hy at a wavelength of 640 nm (frequency = 0.5) for four device structures. As shown in Figure 8a for the Flat device, the power flux is localized around the MEH-PPV emission layer and the ITO layer. On the contrary, the modeled results (Figure 8b−d) show that the incorporation of the 1D grating structure can significantly influence the optical field distribution. The simulation results provide theoretical support to the enhancement of light out-coupling as well as the device efficiency, which is induced by not only the ordinary Bragg scattering but also the combination of the GMR and SPP modes and the hybrid anticross coupling between GMR and SPP. As discussed above (Figure 5), the enhancement ratio of the p-MEH-PPV device is obviously lower than the double-pattern device. The near-field Hy distribution in Figure 8c further identified that such a lower enhancement in the p-MEH-PPV device is due to the absence of Bragg scattering from PEDOT:PSS grating and the hybrid coupling of GMR and SPPs.

4. CONCLUSIONS

In conclusion, we have demonstrated a simple and versatile method to incorporate a well-designed 1D Bragg grating into PLEDs by soft-nanoimprinting lithography, leading to the drastic enhancement the light extraction of trapped optical modes. The resulting efficiency is 1.35 times that of a conventional device with a flat architecture used as a comparison. The experimental characterization and theoretical modeling verify that the enhanced out-coupling efficiency is attributed to the combination of the ordinary Bragg scattering, the GMR and SPP modes, and the hybrid anticross coupling between GMR and SPP, leading to the extraordinary efficient photo flux that can transfer in direction of the leaky modes. This work provides an effective way to liberate the photons flux trapped within the PLEDs. We anticipate that the method described here could also be applied to a wider selection of materials for the production of high-performance PLEDs due to the ease of use and a substantial increase in efficiency.

■ ASSOCIATED CONTENT

Ⓢ Supporting Information

Basic information about simulation of the wavelength-dependent extraordinary optical absorption enhancement for different grating parameters, atomic force microscopy (AFM) image of photoresist on glass substrate, external quantum efficiency as a function of luminance for various devices on ITO coated glass, haze values for different layers on ITO-glass substrates, and the measured complex refractive indices of MEH-PPV, PEDOT:PSS with n and k representing the real and imaginary parts. This material is available free of charge via the Internet at http://pubs.acs.org/.

■ AUTHOR INFORMATION

Corresponding Authors
*Email: jxtang@suda.edu.cn.
*Email: yqli@suda.edu.cn.

Author Contributions
The manuscript was written through contributions of all authors. All authors have given approval to the final version of the manuscript.

Notes
The authors declare no competing financial interest.

■ REFERENCES

(1) Friend, R. H.; Gymer, R. W.; Holmes, A. B.; Burroughes, J. H.; Marks, R. N.; Taliani, C. D. D. C.; Salaneck, W. R. Electroluminescence in Conjugated Polymers. *Nature* **1999**, *397*, 121−128.
(2) D'Andrade, B. W.; Forrest, S. R. White Organic Light-Emitting Devices for Solid-State Lighting. *Adv. Mater.* **2004**, *16*, 1585−1595.

18144

dx.doi.org/10.1021/am5050357 | *ACS Appl. Mater. Interfaces* 2014, 6, 18139−18146

(3) Mandlik, P.; Han, L.; Wagner, S.; Silvernail, J. A.; Ma, R. Q.; Hack, M.; Brown, J. J. A Single-Layer Permeation Barrier for Organic Light-Emitting Displays. *Appl. Phys. Lett.* **2008**, *92*, 103309.

(4) Uoyama, H.; Goushi, K.; Shizu, K.; Nomura, H.; Adachi, C. Highly Efficient Organic Light-Emitting Diodes from Delayed Fluorescence. *Nature* **2012**, *492*, 234−238.

(5) Sun, Y.; Giebink, N. C.; Kanno, H.; Ma, B.; Thompson, M. E.; Forrest, S. R. Management of Singlet and Triplet Excitons for Efficient White Organic Light-Emitting Devices. *Nature* **2006**, *440*, 908−912.

(6) Tsutsui, T.; Yahiro, M.; Yokogawa, H.; Kawano, K.; Yokoyama, M. Doubling Coupling-Out Efficiency in Organic Light-Emitting Devices Using a Thin Silica Aerogel Layer. *Adv. Mater.* **2001**, *13*, 1149−1152.

(7) Hobson, P. A.; Wedge, S.; Wasey, J. A.; Sage, I.; Barnes, W. L. Surface Plasmon Mediated Emission from Organic Light-Emitting Diodes. *Adv. Mater.* **2002**, *14*, 1393−1396.

(8) Bi, Y. G.; Feng, J.; Li, Y. F.; Jin, Y.; Liu, Y. F.; Chen, Q. D.; Sun, H. B. Enhanced Efficiency of Organic Light-Emitting Devices with Metallic Electrodes by Integrating Periodically Corrugated Structure. *Appl. Phys. Lett.* **2012**, *100*, 053304.

(9) Yang, J. P.; Bao, Q. Y.; Xu, Z. Q.; Li, Y. Q.; Tang, J. X.; Shen, S. Light Out-Coupling Enhancement of Organic Light-Emitting Devices with Microlens Array. *Appl. Phys. Lett.* **2010**, *97*, 223303.

(10) Wrzesniewski, E.; Eom, S. H.; Cao, W.; Hammond, W. T.; Lee, S.; Douglas, E. P.; Xue, J. Enhancing Light Extraction in Top-Emitting Organic Light-Emitting Devices Using Molded Transparent Polymer Microlens Arrays. *Small* **2012**, *8*, 2647−2651.

(11) Yamasaki, T.; Sumioka, K.; Tsutsui, T. Organic Light-Emitting Device with an Ordered Monolayer of Silica Microspheres as a Scattering Medium. *Appl. Phys. Lett.* **2000**, *76*, 1243−1245.

(12) Kim, H. K.; Cho, S. H.; Oh, J. R.; Lee, Y. H.; Lee, J. H.; Lee, J. G.; Do, Y. R. Highly Efficient Phosphor-Converted White Organic Light-Emitting Diodes with Moderate Microcavity and Light-Recycling Filters. *Org. Electron.* **2010**, *11*, 137−145.

(13) Bai, Y.; Feng, J.; Liu, Y. F.; Song, J. F.; Simonen, J.; Jin, Y.; Sun, H. B. Outcoupling of Trapped Optical Modes in Organic Light-Emitting Devices with One-Step Fabricated Periodic Corrugation by Laser Ablation. *Org. Electron.* **2011**, *12*, 1927−1935.

(14) Agrawal, M.; Sun, Y.; Forrest, S. R.; Peumans, P. Enhanced Outcoupling from Organic Light-Emitting Diodes Using Aperiodic Dielectric Mirrors. *Appl. Phys. Lett.* **2007**, *90*, 241112.

(15) Sun, Y.; Forrest, S. R. Enhanced Light Out-Coupling of Organic Light-Emitting Devices Using Embedded Low-Index Grids. *Nat. Photonics* **2008**, *2*, 483−487.

(16) Do, Y. R.; Kim, Y. C.; Song, Y. W.; Lee, Y. H. Enhanced Light Extraction Efficiency from Organic Light Emitting Diodes by Insertion of a Two-Dimensional Photonic Crystal Structure. *J. Appl. Phys.* **2004**, *96*, 7629−7636.

(17) Kim, Y. C.; Do, Y. R. Nanohole-Templated Organic Light-Emitting Diodes Fabricated Using Laser-Interfering Lithography: Moth-Eye Lighting. *Opt. Express* **2005**, *13*, 1598−1603.

(18) Zhou, L.; Ou, Q. D.; Chen, J. D.; Shen, S.; Tang, J. X.; Li, Y. Q.; Lee, S. T. Light Manipulation for Organic Optoelectronics Using Bio-Inspired Moth's Eye Nanostructures. *Sci. Rep.* **2014**, *4*, 4040.

(19) Koo, W. H.; Jeong, S. M.; Araoka, F.; Ishikawa, K.; Nishimura, S.; Toyooka, T.; Takezoe, H. Light Extraction from Organic Light-Emitting Diodes Enhanced by Spontaneously Formed Buckles. *Nat. Photonics* **2010**, *4*, 222−226.

(20) Hauss, J.; Bocksrocker, T.; Riedel, B.; Geyer, U.; Lemmer, U.; Gerken, M. Metallic Bragg-Gratings for Light Management in Organic Light-Emitting Devices. *Appl. Phys. Lett.* **2011**, *99*, 103303.

(21) Feng, J.; Okamoto, T.; Kawata, S. Enhancement of Electro-luminescence through a Two-Dimensional Corrugated Metal Film by Grating-Induced Surface-Plasmon Cross Coupling. *Opt. Lett.* **2005**, *30*, 2302−2304.

(22) Wedge, S.; Wasey, J. A. E.; Barnes, W. L.; Sage, I. Coupled Surface Plasmon-Polariton Mediated Photoluminescence from a Top-Emitting Organic Light-Emitting Structure. *Appl. Phys. Lett.* **2004**, *85*, 182−184.

(23) Zhang, S.; Turnbull, G. A.; Samuel, I. D. Enhancing the Emission Directionality of Organic Light-Emitting Diodes by Using Photonic Microstructures. *Appl. Phys. Lett.* **2013**, *103*, 213302.

(24) Liu, G. L.; Lee, L. P. Nanowell Surface Enhanced Raman Scattering Arrays Fabricated by Soft-Lithography for Label-Free Biomolecular Detections in Integrated Microfluidics. *Appl. Phys. Lett.* **2005**, *87*, 074101.

(25) Yang, Y.; Mielczarek, K.; Aryal, M.; Zakhidov, A.; Hu, W. Nanoimprinted Polymer Solar Cell. *ACS Nano* **2012**, *6*, 2877−2892.

(26) Ouyang, J.; Guo, T. F.; Yang, Y.; Higuchi, H.; Yoshioka, M.; Nagatsuka, T. High-Performance, Flexible Polymer Light-Emitting Diodes Fabricated by a Continuous Polymer Coating Process. *Adv. Mater.* **2002**, *14*, 915.

(27) Liu, C.; Kamaev, V.; Vardeny, Z. V. Efficiency Enhancement of an Organic Light-Emitting Diode with a Cathode Forming Two-Dimensional Periodic Hole Array. *Appl. Phys. Lett.* **2005**, *86*, 143501.

(28) Oulton, R. F.; Sorger, V. J.; Genov, D. A.; Pile, D. F. P.; Zhang, X. A Hybrid Plasmonic Waveguide for Subwavelength Confinement and Long-Range Propagation. *Nat. Photonics* **2008**, *2*, 496−500.

(29) Zhou, W.; Wu, Y.; Yu, M.; Hao, P.; Liu, G.; Li, K. Extraordinary Optical Absorption Based on Guided-Mode Resonance. *Opt. Lett.* **2013**, *38*, 5393−5396.

(30) Jin, Y.; Feng, J.; Zhang, X. L.; Bi, Y. G.; Bai, Y.; Chen, L.; Sun, H. B. Solving Efficiency-Stability Tradeoff in Top-Emitting Organic Light-Emitting Devices by Employing Periodically Corrugated Metallic Cathode. *Adv. Mater.* **2012**, *24*, 1187−1191.

(31) Lee, C.; Kim, J. J. Enhanced Light Out-Coupling of OLEDs with Low Haze by Inserting Randomly Dispersed Nanopillar Arrays Formed by Lateral Phase Separation of Polymer Blends. *Small.* **2003**, *9*, 3858−3863.

(32) Koo, W. H.; Zhe, Y.; So, F. Direct Fabrication of Organic Light-Emitting Diodes on Buckled Substrates for Light Extraction. *Adv. Optical Mater.* **2013**, *1*, 404−408.

(33) Ziebarth, J. M.; Saafir, A. K.; Fan, S.; McGehee, M. D. Extracting Light from Polymer Light-Emitting Diodes Using Stamped Bragg Gratings. *Adv. Funct. Mater.* **2004**, *14*, 451−456.

(34) Nguyen, T. Q.; Martini, I. B.; Liu, J.; chwartz, B. J. Controlling Interchain Interactions in Conjugated Polymers: The Effects of Chain Morphology on Exciton-Exciton Annihilation and Aggregation in MEH-PPV Films. *J. Phys. Chem. B* **2000**, *104*, 237−255.

(35) Ha, Y. G.; You, E. A.; Kim, B. J.; Choi, J. H. Fabrication and Characterization of OLEDs Using MEH-PPV and SWCNT Nano-composites. *Synth. Met.* **2005**, *153*, 205−208.

(36) Geyer, U.; Hauss, J.; Riedel, B.; Gleiss, S.; Lemmer, U.; Gerken, M. Large-Scale Patterning of Indium Tin Oxide Electrodes for Guided Mode Extraction from Organic Light-Emitting Diodes. *J. Appl. Phys.* **2008**, *104*, 093111.

(37) Jeong, S. M.; Araoka, F.; Machida, Y.; Takanishi, Y.; Ishikawa, K.; Takezoe, H.; Suzaki, G. Enhancement of Light Extraction from Organic Light-Emitting Diodes with Two-Dimensional Hexagonally Nanoimprinted Periodic Structures Using Sequential Surface Relief Grating. *Jpn. J. Appl. Phys.* **2008**, *47*, 4566.

(38) Lupton, J. M.; Matterson, B. J.; Samuel, I. D.; Jory, M. J.; Barnes, W. L. Bragg Scattering from Periodically Microstructured Light Emitting Diodes. *Appl. Phys. Lett.* **2000**, *77*, 3340−3342.

(39) Choy, W. C.; Ho, C. Y. Improving the Viewing Angle Properties of Microcavity OLEDs by Using Dispersive Gratings. *Opt. Express* **2007**, *15*, 13288−13294.

(40) Do, Y. R.; Kim, Y. C.; Song, Y. W.; Cho, C. O.; Jeon, H.; Lee, Y. J.; Lee, Y. H. Enhanced Light Extraction from Organic Light-Emitting Diodes with 2D SiO_2/SiN_x Photonic Crystals. *Adv. Mater.* **2003**, *15*, 1214−1218.

(41) Zhang, X. L.; Feng, J.; Song, J. F.; Li, X. B.; Sun, H. B. Grating Amplitude Effect on Electroluminescence Enhancement of Corrugated Organic Light-Emitting Devices. *Opt. Lett.* **2011**, *36*, 3915−3917.

(42) Hauss, J.; Bocksrocker, T.; Riedel, B.; Lemmer, U.; Gerken, M. On the Interplay of Waveguide Modes and Leaky Modes in Corrugated OLEDs. *Opt. Express* **2011**, *19*, A851−A858.

(43) Bian, Y.; Zheng, Z.; Zhao, X.; Liu, L.; Su, Y.; Xiao, J.; Zhou, T. Dielectrics Covered Metal Nanowires and Nanotubes for Low-Loss Guiding of Subwavelength Plasmonic Modes. *J. Lightwave Technol.* **2013**, *31*, 1973−1979.

(44) Sakat, E.; Vincent, G.; Ghenuche, P.; Bardou, N.; Collin, S.; Pardo, F.; Haïdar, R. Guided Mode Resonance in Subwavelength Metallodielectric Free-Standing Grating for Bandpass Filtering. *Opt. Lett.* **2011**, *36*, 3054−3056.

(45) Cho, E. H.; Kim, H. S.; Cheong, B. H.; Oleg, P.; Xianyua, W.; Sohn, J. S.; Park, Y. P. Two-Dimensional Photonic Crystal Color Filter Development. *Opt. Lett.* **2009**, *17*, 8621−8629.

(46) Liu, H.; Sun, X.; Pei, Y.; Yao, F.; Jiang, Y. Enhanced Magnetic Response in a Gold Nanowire Pair Array through Coupling with Bloch Surface Waves. *Opt. Lett.* **2011**, *36*, 2414−2416.

(47) Fuchs, C.; Schwab, T.; Roch, T.; Eckardt, S.; Lasagni, A.; Hofmann, S.; Scholz, R. Quantitative Allocation of Bragg Scattering Effects in Highly Efficient OLEDs Fabricated on Periodically Corrugated Substrates. *Opt. Express* **2013**, *21*, 16319−16330.

(48) Jang, J. H.; Oh, M. C.; Yoon, T. H.; Kim, J. C. Polymer Grating Imbedded Organic Light Emitting Diodes with Improved Out-Coupling Efficiency. *Appl. Phys. Lett.* **2010**, *97*, 123302.